Journal of
Instrumentation

PAPER • OPEN ACCESS

Position reconstruction of heavy-ion interactions in plastic scintillator detectors

To cite this article: H.M. Albers and M. Polettini 2026 *JINST* **21** P01024

Published by IOP Publishing for Sissa Medialab

Received: *July 23, 2025*
Revised: *November 1, 2025*
Accepted: *December 19, 2025*
Published: *January 21, 2026*

Position reconstruction of heavy-ion interactions in plastic scintillator detectors

H.M. Albers[a,*] **and M. Polettini**[b,a]

[a] *GSI Helmholtzzentrum für Schwerionenforschung GmbH, Planckstrasse 1, 64291 Darmstadt, Germany*
[b] *Facility for Antiproton and Ion Research in Europe GmbH (FAIR GmbH), Planckstrasse 1, 64291 Darmstadt, Germany*

E-mail: h.albers@gsi.de

Abstract: Active stoppers in the field of low-energy nuclear spectroscopy are detector systems wherein both radioactive ions and their decay products are measured. Information regarding the time and the position of the interactions is needed in order to correlate the daughter radiation with its parent such that physical properties of the decaying system can be obtained. Whereas silicon-based technologies (e.g. segmented double-sided silicon strip detectors) are well established for this use, they exhibit a limited timing resolution that prohibit fast-timing measurements of nuclear states fed by β or α decay. The use of detector systems based on organic plastic scintillator material coupled with silicon photomultipiers as active stoppers offers the attractive possibility of providing excellent timing properties for some experimental cases where short-lived excited nuclear states are fed by particle radiation.

In this work, we investigate the position resolution for heavy-ion interactions of the 'βPlast' plastic scintillator detectors developed for use in DESPEC (DEcay SPECtroscopy) experiments at the GSI/FAIR facility. We present a novel method of extracting interaction positions employing k-nearest neighbour, non-generalising search methods using a highly-segmented double-sided silicon strip detector to provide reference samples. A KD-Tree search method with a Euclidean metric yields resolutions of $\sigma_X = 1.43(5)$ mm and $\sigma_Y = 1.27(2)$ mm in the X and Y directions, respectively.

Keywords: Analysis and statistical methods; Scintillators, scintillation and light emission processes (solid, gas and liquid scintillators); Instrumentation for heavy-ion accelerators; Heavy-ion detectors

*Corresponding author.

https://doi.org/10.1088/1748-0221/21/01/P01024

Contents

1 Introduction

Detectors based on organic plastic scintillator materials are widely used across numerous applied scientific fields (e.g. for biomedical, aerospace and agricultural domains) mainly due to their attractive properties for fast-response radiation detection and their low cost compared to alternative solutions. The characteristics of plastic scintillators are also ideally suited to the field of nuclear physics to provide high-efficiency detection of ionising radiation; indeed, almost all modern experimental nuclear physics facilities employ plastic technology (e.g. [1–3]). In addition, the more recent development of silicon photomultipliers (SiPMs), which are compact and operate at relatively low voltages, has enabled the construction of plastic-based detector systems of increasingly complex geometries.

A new generation of scintillating plastic detectors, named 'βPlast', have been developed for DEcay SPECtroscopy (DESPEC) experiments at the GSI Helmholtzzentrum für Schwerionenforschung in Darmstadt, Germany [4]. DESPEC forms part of the NUSTAR (NUclear STructure, Astrophysics and REactions) collaboration, which represents one of the scientific pillars of the FAIR accelerator facility currently entering its commissioning phase in Darmstadt, Germany [5]. The DESPEC detector suite will sit at one of the focal planes of the Super-conducting FRagment Separator [6], where exotic isotopes produced in fragmentation or fission reactions will be delivered with an event-by-event particle identification. Once at the focal plane, the ions of interest will then be stopped at the centre of the DESPEC setup, and subsequent radiative decays (α, β, γ and neutron) will be measured by a variety of different detector configurations depending on the physics goals of the experiment.

Currently, the βPlast detectors are mounted in the DESPEC setup within the so-called 'implantation stack' in combination with double-sided silicon strip detectors (DSSDs) into which the exotic ions are stopped. One of the main goals of the DESPEC collaboration is to measure the lifetimes of excited nuclear states in exotic nuclei, which are directly related to the nuclear matrix elements and can yield key information regarding the underlying nuclear structure. The βPlast detectors were therefore developed to enable fast-timing measurements for β-γ coincidences wherein β particles emitted by

ions that have been implanted into one of the DSSDs are incident on a βPlast detector and the γ radiation is measured by an auxiliary array. This enables the measurement of short nuclear lifetimes that would otherwise be inaccessible due to the limited timing properties of the silicon detectors. Additionally, the βPlast detectors can serve as a useful veto for light ions passing through the setup.

The use of the βPlast detectors as active stoppers (i.e. ions are stopped and measured inside of the plastic material as well as the subsequent decay radiation) would simplify and improve the efficiency of the setup as one would no longer rely on observing decay events that escape another detector system. This is particularly advantageous in the case of α-decaying nuclei, where the short stopping distance of the α particles in silicon precludes the observation of escape events. However, an important prerequisite of an active-stopper system is that the interaction positions must be well known in order to accurately correlate decay products with their parent isotopes in both space and time. Otherwise, only experiments in which the implantation rate is significantly lower than the decay rate of the stopped isotopes could be carried out. The main goal of this work is to determine the position resolution of the βPlast detectors for heavy-ion interactions. Investigation of the resolution for decay events (both α and β particles), which is more challenging due to the lower light yield and longer stopping distances, is the subject of a follow-up work.

2 βPlast detectors

Different βPlast detector configurations have been developed in order to accommodate various geometries of auxiliary detector systems, although the basic working principles of each are the same. The detectors relevant to this work (shown on the left of figure 1) are composed of a single $80 \times 80 \times 3$-mm^3 sheet of type BC-404 scintillating plastic (manufactured by Saint-Gobain Crystals). The four edges of the plastic are coupled using optical glue to 1-dimensional arrays of 3×3-mm^2 SensL C-Series silicon photomultiplers (SiPMs) with a total of 16 SiPMs along each side. The layout of SiPMs on the PCB for a single edge can be seen at the top of figure 1. Groups comprising four adjacent SiPMs are coupled via custom-built PCBs, resulting in a total of 16 readout channels. Detector signals are processed using FPGA-based TAMEX multichannel front-end cards, developed by the GSI Experimental Electronics department, which provide energy information via the signal Time-over-Threshold (ToT) and excellent (~ 20 ps) timing precision. As one of the channels of the TAMEX cards (corresponding to channel 14 of the detector readout) was not functioning during the data collection phase of the work described here, data from a total of 15 channels are considered. A complete technical description of the βPlast detectors is currently in preparation.

3 Experimental methodology and data preparation

3.1 Description of experimental setup

To evaluate how well the interaction positions can be reconstructed, a suitable data set collected under controlled experimental conditions is required in which the true positions are well defined. Such labelled data could be generated using collimated radioactive sources placed at regular intervals on the detector surface, with the advantage that data could be produced easily and in the required quantities. However, disadvantages of this method include difficulties in simulating realistic heavy-ion interactions with sources and additional complexity when applying algorithms developed using

2026 JINST 21 P01024

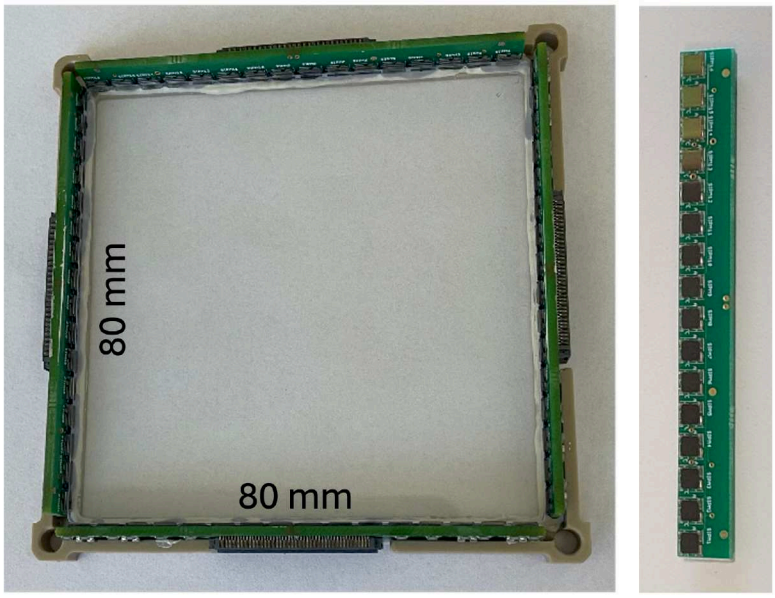

Figure 1. (left) βPlast detector comprising a 3-mm thick sheet of scintillating plastic coupled to SiPMs enclosed in a custom frame constructed via additive manufacturing. (right) PCB layout of one of the four sides of a βPlast detector.

radioactive sources to experimental data collected under different conditions. We have therefore constructed a scheme, described in the following sections, allowing labelled data to be generated in situ with real interactions.

Data were collected during the FAIR Phase-0 program, in which instrumentation developed for the FAIR facility is used at the existing accelerator complex at the GSI Helmholtzzentrum, Germany. A primary beam of ^{238}U ions, accelerated to $\sim$ 1 GeV/u by the SIS-18 synchrotron, collided with a ^{9}Be target to produce heavy ions in fragmentation and fission reactions. Reaction products were transported through the GSI FRagment Separator (FRS) [7], which provided ion-by-ion particle identification according to mass-to-charge ratios (A/Q) and atomic numbers (Z). For further information on the separation and particle-identification methods employed by the FRS, readers are directed to references [7] and [8]. The FRS settings were optimised such that heavy ions with $A \sim 220$–230 and $Z \sim 80$–90 were transmitted to the final focal plane and were incident on the DESPEC implantation stack, where the ions either deposited energy while passing through or were completely stopped, depending on their Z.

The implantation stack comprised layers of βPlast and AIDA (Advanced Implantation Detector Array [9]) detectors, as indicated in the schematic shown in figure 2. The AIDA detectors are highly-pixellated double-sided silicon strip detectors (DSSDs) of dimension 80×80 mm^2 and thickness 1 mm, with a heavy-ion detection efficiency close to 100%. Each DSSD is segmented into 128 strips in both the X and Y directions with a strip pitch of 560 µm. As the distance between detectors within the implantation stack was less than 15 mm, the effect of the angles of the incoming heavy ions was negligible and trajectories could be approximated as orthogonal to the detector surfaces. In this configuration, the position resolution of the upstream βPlast detector (labelled βPlast 1 in figure 2) was investigated using the known positions recorded by the upstream AIDA detector (hereafter referred to as AIDA 1).

2026 JINST 21 P01024

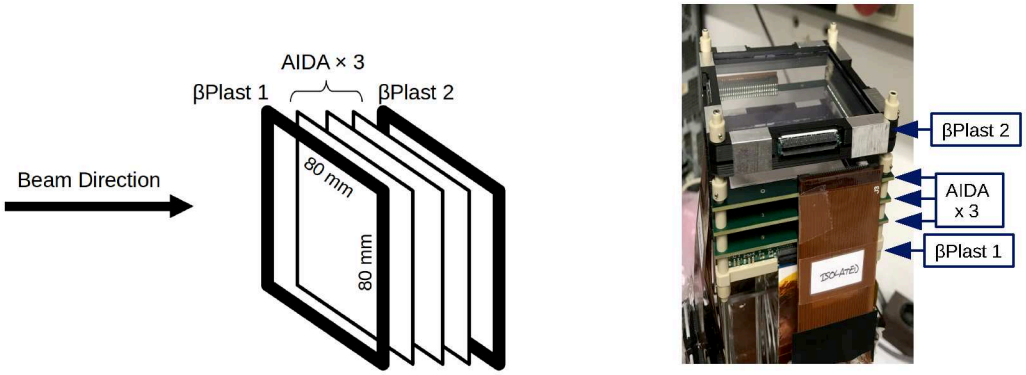

Figure 2. (left) Schematic of the detector layout within the implantation stack. Two βPlast fast scintillator detectors surround three AIDA double-sided silicon strip detectors, with an inter-detector spacing of $\sim$ 10–15 mm. (right) Labelled photograph of the implantation stack containing mounted detectors.

3.2 Data processing and preparation

The three AIDA detectors were read out via a triggerless data acquisition system independent of that of the βPlast detectors. A common 125-MHz clock (the 'White Rabbit' timing system [10]) was used to timestamp data collected from the AIDA and βPlast systems such that coincident events (i.e. events wherein both systems recorded data within a 10-µs window) could be cleanly identified. An additional coincidence between signals registered by the FRS and the βPlast was applied to select events associated with ions transmitted through the separator to the final focal point, where the DESPEC setup was located. The following selection criteria were also implemented:

- Only a single interaction should be registered per event by the AIDA 1 detector. A small number (less than 1%) of events in which more than one interaction position was recorded by AIDA 1 were removed. These events can occur when lighter ions produced in reactions upstream of the detector array are incident on the detector surface in coincidence with the heavy ions.
- As heavy-ion interactions in the scintillation material generate a large amount of light, only events in which all of the βPlast readout channels registered hits were selected. As one of the 16 βPlast readout channels was not functioning during the data collection period, βPlast events with a channel multiplicity of 15 were accepted.

The hit pattern of events passing the selection criteria registered by AIDA 1 is shown in figure 3. Due to the ion-optical settings of the FRS, the beam profile was defocussed in the X direction but rather narrow in the Y direction. Two vertical strips positioned at $X \sim 32$ mm and $X \sim 52$ mm were not functioning properly and therefore recorded little or no heavy-ion interactions.

4 Reconstruction of interaction positions

4.1 Proof of principle

Algorithms based upon so-called 'Anger' (or Centre-Of-Gravity) methods [11], wherein the signal amplitudes are weighted by the detection positions, are commonly used to reconstruct interaction positions in scintillator materials [12]. In the data presented here, the large amount of scintillation

2026 JINST 21 P01024

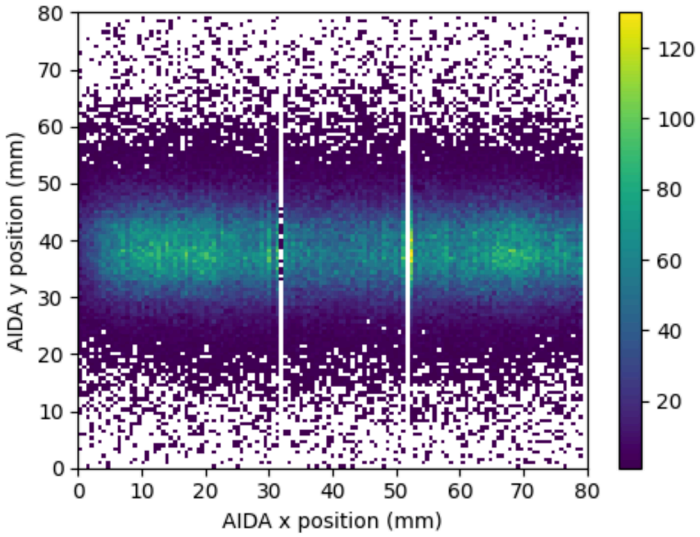

Figure 3. Interaction positions of heavy ions on the AIDA 1 detector.

light produced during the ion interactions leads to saturation of the SiPMs, precluding the use of the energy distributions recorded along the edges of the βPlast detectors to reconstruct the hit positions. The situation is different for lower-energy particle-decay events, which occur within the detector after the implantation of radioactive ions, wherein the resulting energy distribution may indeed be used to reconstruct the decay position. As was previously stated, investigating the achievable position resolution for such particle-decay events is the topic of a separate work.

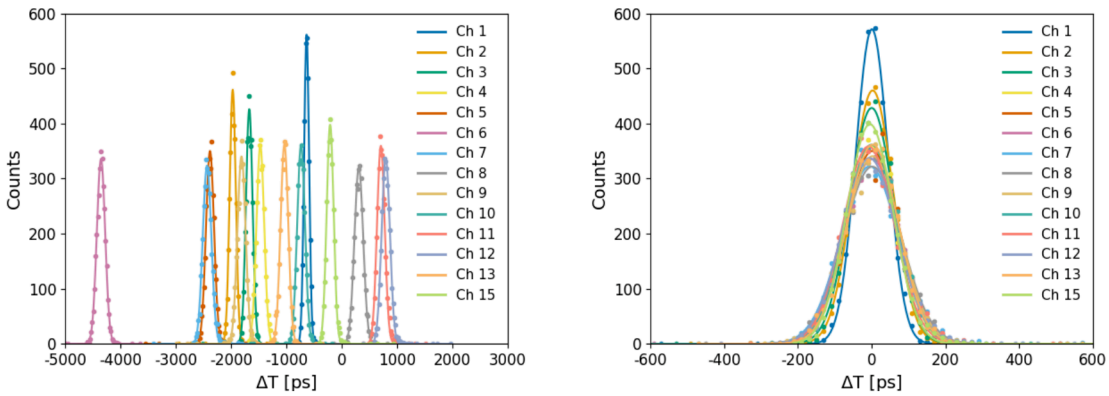

Figure 4. (left) Time differences ΔT between individual channels and reference channel 0 for hits occurring within the central 5×5-mm^2 region of the AIDA 1 detector. (right) As left panel but with alignment parameters applied.

For the data considered here, the time at which the light arrives at the SiPMs is used as input for the reconstruction algorithms. The method is based on the simple principle that light emitted at a larger distance from the SiPMs will take longer to reach them. To test the validity of the method, we first assessed the time differences (ΔT) between each channel and a reference channel (channel 0 was chosen arbitrarily) for events that were registered in the central 5×5-mm^2 region of the AIDA 1 detector. The resulting distributions can be found in the left-hand panel of figure 4. Note that a

2026 JINST 21 P01024

small central region was selected in order to reduce the width of the time-difference distributions by restricting the possible range of path lengths taken by the scintillation photons, and to allow the assumption that the path lengths should be symmetrically distributed about zero. Whereas the shape of the distributions are similar, the centroids are shifted due to variations in the electronic chains and cabling of each βPlast readout channel, which affects the timing properties. To account for this, a constant offset was then added to the ΔT values of each channel such that all ΔT distributions were centered around zero, as shown in the right-hand panel of the same figure. These offsets were then applied to the time differences on an event-by-event basis. The FWHMs of the resulting time distributions are $\sim$ 100-180 ps for single channels and 157.7(2) ps for the sum of all channels.

To demonstrate the reconstruction principle and to gauge the sensitivity of the method, five 5×5-mm^2 regions separated by a distance of 5 mm were defined on the AIDA 1 detector and used to select interactions occurring in the corresponding areas in the βPlast. These regions, labelled G1-G5, are indicated in the sketch of the βPlast channel layout given in the left-hand panel of figure 5. Note that channel 14, from which no data was recorded, is marked with an 'X'.

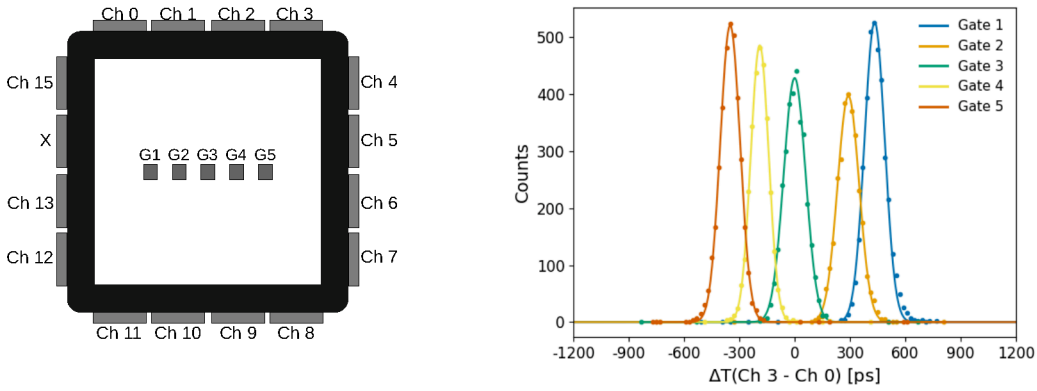

Figure 5. (left) Sketch of βPlast detector channel layout. Squares labelled G1-G5 indicate the $\sim 5 \times 5$-mm^2 regions of the AIDA 1 detector comprising gates 1–5, respectively. Note that channel 14 was not functioning during data collection and is marked 'X'. (right) Time-difference distributions ΔT between channel 3 and channel 0, gated on the 5 regions G1–G5 indicated in the left-hand panel.

The right-hand panel of figure 5 shows the aligned time differences between channel 3 and the reference channel 0 for regions G1–G5. As expected, $\Delta T = T_{\mathrm{Ch3}} - T_{\mathrm{Ch0}} > 0$ for events occurring in region G1 as the scintillation light has a longer path to reach channel 3 compared to channel 0. Similarly, $\Delta T = T_{\mathrm{Ch3}} - T_{\mathrm{Ch0}} < 0$ for events occurring in region G5. Despite the symmetry of the detector layout, the time distributions shown in figure 5 are not symmetric around zero, which could be due to variations in the SiPM characteristics, asymmetries in the experimental layout or inhomogeneities in the scintillation material itself.

4.2 Look-up table method

The method used in this work — the 'look-up table' (LUT) method — is based upon the creation of a data array that maps the βPlast channel time differences to the corresponding known interaction positions measured by the AIDA 1 detector. LUTs were generated from experimental data collected and analysed as described in section 3. The composition of the LUTs is shown in table 1, where StrX

2026 JINST 21 P01024

and StrY are the X and Y strip numbers of the AIDA 1 detector and ΔTi are given by

$$\Delta Ti = T_i - T_0, \quad i = [1, \ldots 13, 15], \tag{4.1}$$

where T_i and T_0 are the timestamps registered by between channel i and reference channel 0, respectively. Average values of ΔTi were calculated in cases where multiple events were recorded for a given (StrX,StrY) combination.

Table 1. Look-up table format.

StrX	StrY	$\Delta T1_{(\mathrm{StrX,StrY})}$	...	$\Delta T15_{(\mathrm{StrX,StrY})}$
0	0	$\Delta T1_{(0,0)}$	...	$\Delta T15_{(0,0)}$
0	1	$\Delta T1_{(0,1)}$	...	$\Delta T15_{(0,1)}$
0	2	$\Delta T1_{(0,2)}$	...	$\Delta T15_{(0,2)}$
⋮	⋮	⋮		
127	125	$\Delta T1_{(127,125)}$	...	$\Delta T15_{(127,125)}$
127	126	$\Delta T1_{(127,126)}$	...	$\Delta T15_{(127,126)}$
127	127	$\Delta T1_{(127,127)}$	...	$\Delta T15_{(127,127)}$

Interaction positions are obtained by comparing the time differences associated with the heavy-ion events of interest with those in the LUT. This is an example of a k-nearest neighbour, non-generalising, machine-learning search method [13], wherein k samples in the LUT closest to the new point of interest are found ($k = 1$ for the case described here where a single sample is chosen). How close a sample is to the new point of interest can be measured by a distance metric d. The two simple metrics used here are Euclidean

$$d_E = \sqrt{\sum_i (\Delta Ti_{\mathrm{test}} - \Delta Ti_{\mathrm{LUT}})^2}, \quad i = [1, \ldots 13, 15] \tag{4.2}$$

and Manhattan

$$d_M = \sum_i |\Delta Ti_{\mathrm{test}} - \Delta Ti_{\mathrm{LUT}}|, \quad i = [1, \ldots 13, 15]. \tag{4.3}$$

A methodology based on k-nearest neighbour search algorithms was successfully employed in the work of Xin Li et al. [14], where γ-ray interaction positions were reconstructed using mean-detector-response-functions for LYSO-based PET scanners in medical applications.

A search wherein d is calculated for every sample in the LUT (the so-called 'brute force' method) will yield a closest match but is computationally intensive and will have a query time that scales as $O[DN]$, where D is the number of features and N is the number of samples. Alternatively, nearest neighbour searches can be carried out by building space-partitioning structures that allow for fast indexing. Commonly-used examples of this include KD Tree [15] and Ball Tree [16] algorithms, allowing closest matches to be found by calculating d for only a subset of all samples. Whereas the query time for Ball Tree algorithms scales approximately as $O[D \log(N)]$, the scaling of the KD Tree algorithm is not trivial to define and is typically efficient for small dimensionality ($D < 20$) but comparable with brute force for large D.

2026 JINST 21 P01024

5 Results and discussion

Data structures were built in a Python framework using the NearestNeighbors class available within the scikit-learn machine-learning library (ref. [17]) using the LUTs as input. An independent dataset comprising 1000 heavy-ion events that were not used in the LUT construction was used to test the methods and extract the achievable position resolution. Values of $\Delta X = X_{\mathrm{TRUE}} - X_{\mathrm{LUT}}$ were calculated for each test event, where X_{TRUE} and X_{LUT} are the X strip numbers of the real interaction positions as recorded by AIDA 1 and the closest-matching sample found in the LUT, respectively. Values of ΔY were calculated similarly.

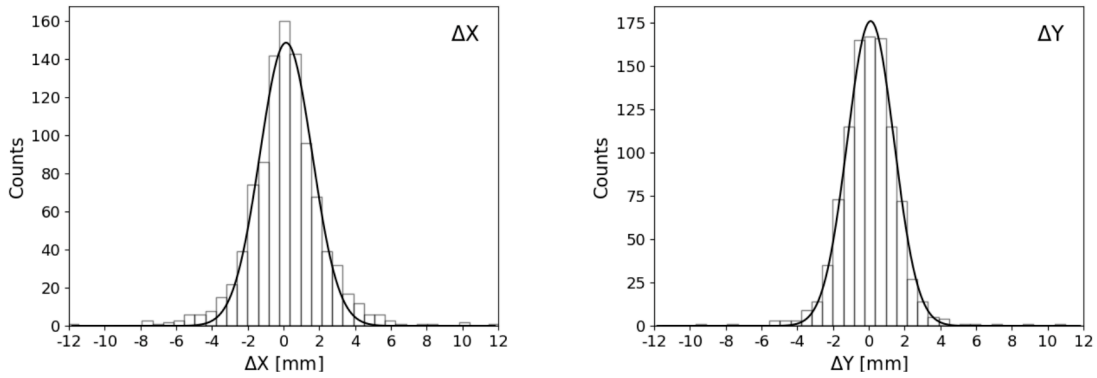

Figure 6. ΔX (left) and ΔY (right) distributions.

Table 2. Position resolutions achieved in both the X and Y directions (σ_X and σ_Y, respectively) using the LUT method.

Num. events in LUT	Distance metric d	σ_X [mm]	σ_Y [mm]
2×10^5	Euclidean	1.43(5)	1.27(2)
5×10^5	Euclidean	1.45(7)	1.17(4)
2×10^5	Manhattan	1.51(5)	1.33(4)
5×10^5	Manhattan	1.55(6)	1.33(4)

The ΔX and ΔY values for the 1000 test events, calculated using the KD Tree algorithm with the Euclidean distance metric using a LUT built using 2×10^5 events, are plotted in the left and right panels of figure 6, respectively. The position resolutions for X and Y (σ_X and σ_Y, respectively), which were extracted as standard deviations from Gaussian fits to the distributions shown as solid black lines in the same figure, are given in table 2. A small improvement in σ_Y could be achieved by increasing the number of events used to construct the LUT from 2×10^5 to 5×10^5 but at the expense of a $\sim 30\%$ longer tree-building time. Additionally, improved results were obtained using the Euclidean metric when compared with the Manhattan, particularly in the Y direction. Values of σ_Y were found to be smaller than for σ_X in all cases, likely due to the very narrow and central distribution of ion events in the y direction (see figure 3). No strong dependency of the resolution on the hit positions was observed, as can be seen in figure 7 where 3-dimensional plots of the absolute values of ΔX and ΔY are shown for different interaction positions on the detector surface.

2026 JINST 21 P01024

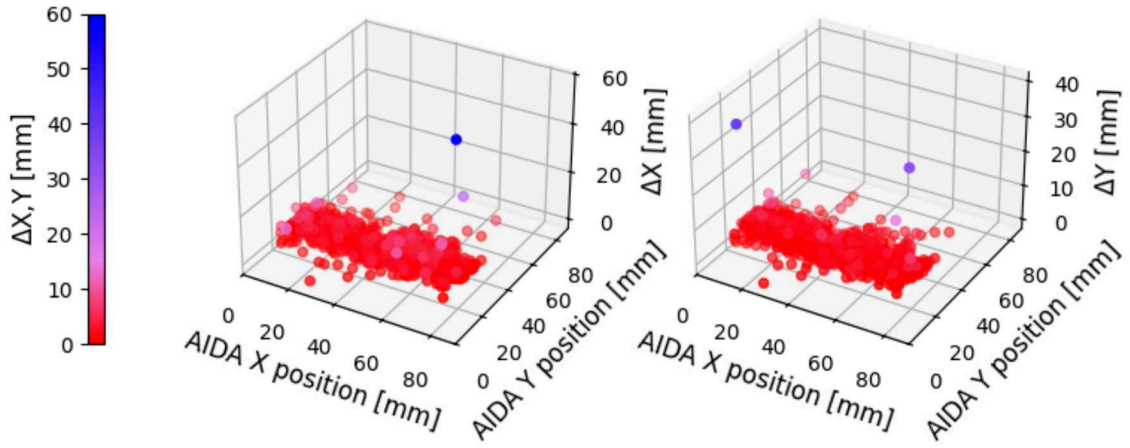

Figure 7. 3-dimensional plots of the absolute values of ΔX (left) and ΔY (right) versus the hit positions recorded by the AIDA 1 detector.

It is clear from figure 7 that, whereas the majority of test events are well reconstructed, a small number of poorly-reconstructed outliers are visible. An advantage of the nearest neighbour search method is that each reconstructed event is associated with a performance metric that can be used to assess how well the closest match resembles the event of interest. The Euclidean distances d_E versus the ΔX and ΔY values can be seen in the left and right panels of figure 8, respectively, where it can been seen that all test events with very large ΔX or ΔY have $d_E > 0.1$. Rejecting matches with $d_E > 0.1$ removes reconstructions wherein no well-matching sample is found.

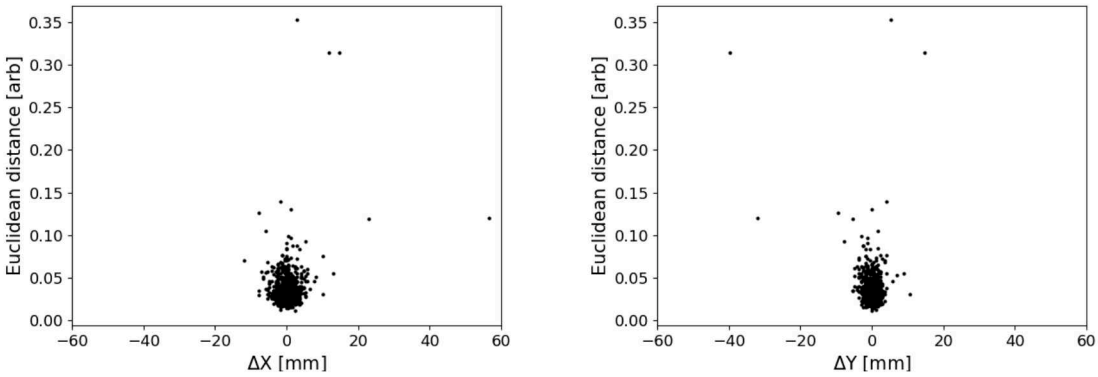

Figure 8. Euclidean distances (d_E) between test events and the corresponding best-matching samples in the look-up table versus ΔX (left) and ΔY (right).

Whereas the σ_X and σ_Y results shown in table 2 are the same for all of the algorithms tested, a comparison of the search execution times for the brute force, KD Tree and Ball Tree algorithms can be found in table 3. Interestingly, the search times, which are normalised to the KD Tree value to account for differences in computing architecture, indicate that the KD Tree search performs the best, but only a moderate improvement compared to the brute force method is exhibited. We also investigated the change in performance when reducing the number of βPlast channels used in the

2026 JINST 21 P01024

LUT samples by considering only odd-numbered channels (i.e. channels 1, 3, . . . , 15 in figure 5). This may be an important consideration for the design of future βPlast detectors as more SiPMs could be combined to a single readout channel thus reducing the cost if resolutions are still within acceptable limits. The results indicate that the resolution is $\sim$ 25% ($\sim$ 30%) worse in the X (Y) directions but that search times are faster for all algorithms.

Table 3. Comparison of search times for brute force, KD Tree and Ball Tree algorithms for all βPlast and only odd-numbered channels using 2×10^5 events in the LUT and a Euclidean metric.

Algorithm	βPlast channels	σ_X [mm]	σ_Y [mm]	Search time [arb]
Brute force	All	1.43(5)	1.27(2)	20.6
KD Tree	All	1.43(5)	1.27(2)	1.0
Ball Tree	All	1.43(5)	1.27(2)	2.8
Brute force	Odd only	1.80(8)	1.66(5)	5.0
KD Tree	Odd only	1.80(8)	1.66(5)	0.7
Ball Tree	Odd only	1.80(8)	1.66(5)	2.0

6 Conclusions and outlook

We have demonstrated that position resolutions of $\sigma < 1.5$ mm can be achieved for interactions in the βPlast plastic scintillators detectors for heavy ions for FAIR Phase-0 DESPEC experiments at GSI (Darmstadt). The novel method, wherein tables of reference samples labelled by positions recorded by a highly-segmented DSSD are searched using k-nearest neighbour algorithms, enables the reference dataset to be collected in situ during experiments.

Several next steps are planned. We will investigate whether the performance can be further improved through the use of artificial neural networks trained on the same data that was used here to construct the LUTs. Additionally, in order to use the βPlasts as active stoppers, the detector capabilities for decay products must be assessed. The performance for α radiation can be evaluated using data collected during DESPEC experiments wherein α-decaying heavy isotopes (with halflives on the order of ms to s) were implanted into one of the βPlast detectors. In this case, the distributions of the energies measured by the SiPMs may be used in addition to the timing signals in order to improve the resolution.

Reconstructing interaction positions for β-decay events presents the largest challenge due to the low energy deposition and long path lengths of the β particles inside of the plastic material as well as difficulties producing clean training datasets. For this purpose, the βPlast detectors will be 'scanned' using the GSI gamma scanning system [18], where Compton-scattered 511-keV annihilation photons can be used to approximate β-particle interactions.

The data presented here was collected using a quadratic $80 \times 80 \times 3$-mm^3 βPlast detector, as described in section 3. In recent years, 'triple' (or 'wide') βPlast detectors of dimension 240×80×3 mm^3 have also been constructed and used during FAIR Phase-0 DESPEC experiments. We plan to extend the methodology presented in this work to the 'wide' detectors to make use of the full focal plane of the FRS (and the future Super-FRS at FAIR) and allow the study of more isotopic species simultaneously.

2026 JINST 21 P01024

Acknowledgments

The results presented here are based on experiment S460, which was performed with the DESPEC setup at the final focal plane of the FRS at the GSI Helmholtzzentrum für Schwerionenforschung, Darmstadt (Germany), in the frame of FAIR Phase-0. The authors would like to give their heartfelt thanks to the accelerator crew at GSI, the members of the FRS beam team and the DESPEC S460 collaboration, who enabled the collection of the data used in the analysis presented here. The publication is funded by the Open Access Publishing Fund of the GSI Helmholtzzentrum für Schwerionenforschung.

References

[1] H. Joukainen, J. Sarén and P. Ruotsalainen, *Position sensitive plastic scintillator for beta particle detection*, *Nucl. Instrum. Meth. A* **1027** (2022) 166253.

[2] C. Neacşu et al., *Development of a plastic scintillator based and SiPM readout detector for high-precision fast-timing measurements at rosphere array*, *Nucl. Instrum. Meth. A* **1065** (2024) 169495.

[3] C. Neacşu et al., *A miniaturized low-power SiPM-based β detector for the ISOLDE Fast Tapestation*, *Nucl. Instrum. Meth. A* **1026** (2022) 166213.

[4] A.K. Mistry et al., *The DESPEC setup for GSI and FAIR*, *Nucl. Instrum. Meth. A* **1033** (2022) 166662.

[5] S. Reimann et al., *FAIR commissioning — Towards first science*, in the proceedings of the *16th International Particle Accelerator Conference*, Taipei, Taiwan, June 1–6 (2025), pp. 2495–2498 [DOI:10.18429/JACoW-IPAC2025-THBN2] [arXiv:2510.14948].

[6] H. Geissel et al., *The Super-FRS project at GSI*, *Nucl. Instrum. Meth. B* **204** (2003) 71.

[7] H. Geissel et al., *The GSI projectile fragment separator (FRS): A versatile magnetic system for relativistic heavy ions*, *Nucl. Instrum. Meth. B* **70** (1992) 286.

[8] G. Munzenberg, *The separation techniques for secondary beams*, *Nucl. Instrum. Meth.* **70** (1992) 265.

[9] O. Hall et al., *The Advanced Implantation Detector Array (AIDA)*, *Nucl. Instrum. Meth. A* **1050** (2023) 168166.

[10] D. Beck et al., *The General Machine Timing System for FAIR and GSI*, https://wiki.gsi.de/pub/TOS/Timing/TimingSystemDocuments/GMT_Description_v3-1.pdf.

[11] H.O. Anger, *Scintillation Camera*, *Rev. Sci. Instrum.* **29** (1958) 27.

[12] A. Ebrahimi et al., *Position reconstruction for segmented detectors*, *Nucl. Instrum. Meth. A* **1014** (2021) 165744 [arXiv:2107.06600].

[13] J. Goldberger, G.E. Hinton, S. Roweis and R.R. Salakhutdinov, *Neighbourhood Components Analysis*, in *Advances in Neural Information Processing Systems*, L. Saul et al. eds., MIT Press (2004), vol. 17, pp. 505–512.

[14] X. Li, L. Tao, C.S. Levin and L.R. Furenlid, *Fast gamma-ray interaction-position estimation using k-d tree search*, *Phys. Med. Biol.* **64** (2019) 155018.

[15] J.L. Bentley, *Multidimensional binary search trees used for associative searching*, *Commun. ACM* **18** (1975) 509.

[16] S. M. Omohundro, *Five Balltree Construction Algorithms*, ICSI Technical Report TR-89-063, ICSI, Berkeley, CA, U.S.A. (1989).

[17] F. Pedregosa et al., *Scikit-learn: Machine Learning in Python*, *J. Mach. Learn. Res.* **12** (2011) 2825 [arXiv:1201.0490].

[18] T. Habermann et al., *Application of gamma imaging techniques for the characterisation of position sensitive gamma detectors*, *Nucl. Instrum. Meth. A* **873** (2017) 24.

2026 JINST 21 P01024